Molecular Cancer Therapeutics

Optimization of a PEGylated Glucuronide-Monomethylauristatin E Linker for Antibody–Drug Conjugates

Patrick J. Burke, Joseph Z. Hamilton, Scott C. Jeffrey, Joshua H. Hunter, Svetlana O. Doronina, Nicole M. Okeley, Jamie B. Miyamoto, Martha E. Anderson, Ivan J. Stone, Michelle L. Ulrich, Jessica K. Simmons, Erica E. McKinney, Peter D. Senter, and Robert P. Lyon

Abstract

The emergence of antibody–drug conjugates (ADC), such as brentuximab vedotin and ado-trastuzumab emtansine, has led to increased efforts to identify new payloads and develop improved drug-linker technologies. Most antibody payloads impart significant hydrophobicity to the ADC, resulting in accelerated plasma clearance and suboptimal *in vivo* activity, particularly for conjugates with high drug-to-antibody ratios (DAR). We recently reported on the incorporation of a discrete PEG_{24} polymer as a side chain in a β-glucuronidase-cleavable monomethylauristatin E (MMAE) linker to provide homogeneous DAR 8 conjugates with decreased plasma clearance and increased antitumor activity in xenograft models relative to a non-PEGylated control. In this work, we optimized the drug-linker by minimizing the size of the PEG side chain and incorporating a self-stabilizing maleimide to prevent payload de-conjugation *in vivo*. Multiple PEG-glucuronide-MMAE linkers were prepared with PEG size up to 24 ethylene oxide units, and homogeneous DAR 8 ADCs were evaluated. A clear relationship was observed between PEG length and conjugate pharmacology when tested *in vivo*. Longer PEG chains resulted in slower clearance, with a threshold length of PEG_8 beyond which clearance was not impacted. Conjugates bearing PEG of sufficient length to minimize plasma clearance provided a wider therapeutic window relative to faster clearing conjugates bearing shorter PEGs. A lead PEGylated glucuronide-MMAE linker was identified incorporating a self-stabilizing maleimide and a PEG_{12} side chain emerged from these efforts, enabling highly potent, homogeneous DAR 8 conjugates and is under consideration for future ADC programs. *Mol Cancer Ther; 16(1); 116–23. ©2016 AACR.*

Introduction

Antibody–drug conjugates (ADC) seek to combine the exquisite specificity of an antibody to its cognate antigen with the cytotoxic potency of the drug payload. Advances in ADC technology have paved the way for two FDA-approved ADCs: CD30-targeted brentuximab vedotin for relapsed and refractory Hodgkin lymphoma and ALCL (1), and HER2-targeted ado-trastuzumab emtansine for HER2-expressing breast cancer (2). There are many design factors crucial to the development of effective ADCs (3–5), and plasma pharmacokinetics has emerged as an important parameter on ADC pharmacology (6).

Payload conjugation to antibodies can impart significant hydrophobicity to the resulting conjugate, which can lead to ADC aggregation and/or accelerated plasma clearance *in vivo*, often limiting the drug-to-antibody ratio. As a consequence, the majority of ADCs in clinical development are loaded with an average of only 2 to 4 drugs per antibody (7). This limitation is due not only to the intrinsically hydrophobic character of the cytotoxic agent used as the drug payload, such as the antimitotic monomethylauristatin E (MMAE) in Fig. 1, but also to the linker technology employed to ensure the release of the drug in a chemically unmodified form. For example, self-immolative cleavable linker systems like the valine-citrulline (val-cit) dipeptide (drug-linker **1**) and glucuronides (drug-linkers **2**–**10**) rely on a [1,6]-fragmentation across a hydrophobic aryl spacer to achieve drug release, adding additional hydrophobicity to the conjugate. Recently, we reported that a DAR 8 ADC prepared with the hydrophobic drug-linker val-cit-monomethylauristatin F was taken up by Kupffer cells and hepatic sinusoidal endothelial cells, likely contributing to the accelerated plasma clearance in rats (6). This uptake was greatly diminished when using drug-linkers designed to minimize hydrophobicity, and the resulting ADCs exhibited plasma pharmacokinetics similar to that of the unconjugated antibody.

Although an effective drug-linker for ADCs (8), drug-linker **1** (Fig. 1) has limitations. The physicochemical properties of the drug-linker limit the optimal drug-loading to approximately 4 drugs per antibody when conjugated as a distribution across four reducible native antibody cysteine disulfides. Early work with drug-linker **1** demonstrated that higher loaded DAR 8 conjugates, while more potent than lower loaded ADCs *in vitro*, were inferior *in vivo* due to accelerated plasma clearance (9). In this work, we sought to achieve greater ADC potency and homogeneous DAR 8 conjugates by stably conjugating MMAE via a hydrophilic PEGylated glucuronide linker system.

Seattle Genetics, Inc., 21823 30th Drive SE, Bothell, Washington.

Note: Supplementary data for this article are available at Molecular Cancer Therapeutics Online (http://mct.aacrjournals.org/).

Corresponding Author: Patrick J. Burke, Seattle Genetics, Inc., 21823 30th Drive SE, Bothell, WA 98021. Phone: 425-527-4766; Fax: 425-527-4109; E-mail: pburke@seagen.com

doi: 10.1158/1535-7163.MCT-16-0343

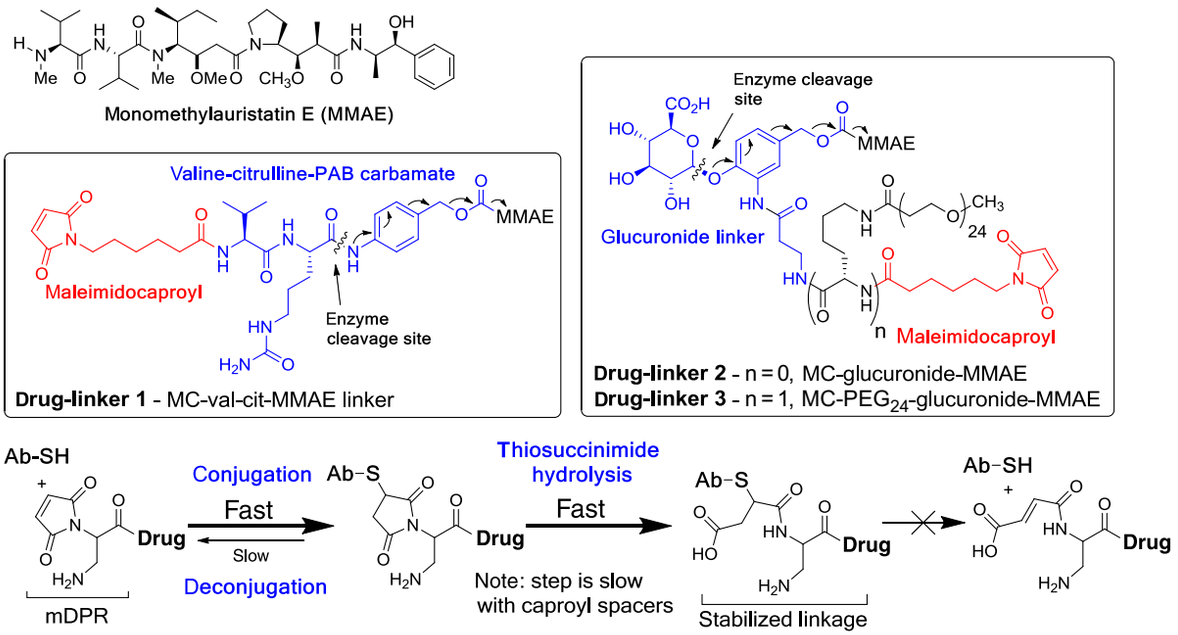

Figure 1.
Structures of monomethylauristatin E drug-linkers and self-stabilizing maleimide (mDPR).

The glucuronide linker system represents a hydrophilic alternative to the val-cit dipeptide, and exploits lysosomal β-glucuronidase (10) to initiate drug release. The glucuronide linker has been used to mitigate aggregation issues with lipophilic payloads like minor groove binders (11) and camptothecins (12). Glucuronide-MMAE linker **2** was found to provide ADCs at 4-drugs/Ab with *in vitro* and *in vivo* properties similar to val-cit-MMAE linker **1** conjugates (13). More recently, we have shown that incorporation of a PEG_{24} solubilizing moiety in a side chain configuration (drug-linker **3**), but not as a tether between the maleimide and drug, enabled ADCs loaded at 8-drugs/Ab with greater plasma exposure and improved *in vivo* performance relative to non-PEGylated drug-linker **2** controls (6).

A second limitation of drug-linker **1** is the utilization of the maleimidocaproyl (MC) stretcher unit for covalent attachment of the drug-linker to the targeting antibody. Simple alkyl maleimides are known (14) to undergo partial de-conjugation *in vivo*, as the reaction of the Cys thiol with the maleimide is reversible and *in vivo* the drug-linker maleimide can be captured by endogenous albumin (ref.14; Fig. 1). Once the thiosuccinimide product of the maleimide conjugation undergoes ring hydrolysis, however, the covalent linkage of the drug-linker to the antibody is stabilized. The self-stabilizing maleimide (mDPR; Fig. 1) was developed to undergo rapid postconjugation thiosuccinimide hydrolysis, to provide circulation-stable ADCs with a wider therapeutic window (15).

The goal of this work was to optimize conjugate delivery of MMAE by combining these advancements to maximize ADC potency and therapeutic window from homogeneous DAR 8 conjugates. Specifically, we sought to optimize drug-linker **3** through incorporation of the mDPR self-stabilizing maleimide and investigate the effects of PEG length on pharmacological properties.

Materials and Methods

Preparation of ADCs bearing mDPR-PEG_x-glucuronide-MMAE linkers

A detailed experimental procedure for the preparation of the drug-linkers has been previously described (6, 16). Anti-CD30 and anti-CD19 antibodies, cAC10 and hBU12, respectively, were conjugated as previously described (17). Briefly, a solution of antibody around 10 mg/mL in PBS (pH 7.4) containing 1 mmol/L EDTA was treated with 12 equivalents of tris(2-carboxy-ethyl)-phosphine (TCEP) to achieve full reduction of the four interchain disulfides. Reduction progress was monitored by reversed-phase chromatography and additional TCEP was added as needed to complete the reaction. Upon reaction completion, the reduced antibody solution was purified by three rounds of 10-fold dilution and centrifugation at 4,000 × *g* through a 30-kDa molecular weight cutoff (MWCO) filter.

Fully reduced antibody as a PBS solution containing 1 mmol/L EDTA and buffered with 100 mmol/L potassium phosphate to pH 7.4 was conjugated with 10 molar equivalents (25% excess) of drug-linker as a 10 mmol/L DMSO stock. The resulting solution was vortexed and left at room temperature for 15 to 30 minutes. The extent of conjugation was assessed by reversed-phase chromatography and additional drug-linker was added as needed. Once all eight available mAb cysteines were alkylated, the crude ADC solution was purified by three rounds of 10-fold dilution with PBS and centrifugation at 4,000 × *g* through a 30-kDa MWCO filter. The extent of aggregation was assessed by size exclusion chromatography (SEC), and in all cases, monomeric ADCs were obtained with less than 2% aggregation. The SEC chromatograms revealed a shift to shorter retention times as the PEG length in the drug-linker increased, indicative of an increase in apparent ADC size (Supplementary Fig. S1). The resulting DAR

8 homogeneous ADCs were sterile-filtered through a 0.22-μm centrifugal filter and stored at −80°C.

In vitro cytotoxicity assays

In vitro potency was assessed on multiple cancer cell lines: L540cy and L428 (Hodgkin lymphomas); Karpas299 (anaplastic large cell lymphoma, originally provided by Dr. Abraham Karpas, University of Cambridge, Cambridge, UK), Ramos (Burkitt lymphoma), and SU-DHL-4, WSU-DLCL2, and RL (diffuse large B-cell lymphoma) cell lines. L428, Karpas299, SU-DHL-4, and WSU-DLCL2 cell lines were obtained from DSMZ. Ramos and RL cell lines were obtained from ATCC. The L540cy cell line was provided by Dr. Harald Stein (Institut fur Pathologie, University of Veinikum Benjamin Franklin, Berlin, Germany). The $CD30^+$ Karpas299, L540cy, and L428 lymphoma cell lines were obtained in 2012. The $CD19^+$ Ramos, SU-DHL-4, WSU-DLCL2, and RL lymphoma cell lines were obtained in 2013. All cell lines were authenticated by STR profiling at IDEXX Bioresearch and cultured for no more than 2 months after resuscitation. Cells cultured in log-phase growth were seeded for 24 hours in 96-well plates containing 150-μL RPMI1640 supplemented with 20% FBS. Serial dilutions of ADCs in cell culture media were prepared at 4× working concentrations, and 50 μL of each dilution was added to the 96-well plates. Following addition of ADC, cells were incubated with test articles for 4 days at 37°C, after which growth inhibition was assessed by CellTiter-Glo (Promega). The EC_{50} value, determined in triplicate, is defined as the concentration that achieves half-maximal growth inhibition over the course of the titration curve.

In vivo tolerability and therapy experiments

All experiments were conducted in concordance with the Institutional Animal Care and Use Committee in a facility fully accredited by the Association for Assessment and Accreditation of Laboratory Animal Care. To assess mouse tolerability, Balb/C mice ($n = 3$) were treated with a single intraperitoneal dose of 50 mg/kg of ADC on day 0. The mice were then observed for weight loss or outward signs of toxicity over the course of nine days. Mice experiencing greater than 20% weight loss were euthanized.

Efficacy experiments were conducted in CD19-expressing RL and WSU-DLCL2 models of diffuse large B-cell lymphoma (DLBCL) and the Raji model of Burkitt lymphoma. Tumor cells, as a suspension, were implanted subcutaneously in immune-compromised SCID mice. Upon tumor engraftment, mice were randomized to study groups when the average tumor volume reached about 100 mm^3. Test articles were administered once via intraperitoneal bolus injection. Tumor volume as a function of time was determined using the formula $(L \times W^2)/2$. Animals were euthanized when tumor volumes reached 1,000 mm^3.

Intratumoral concentration of MMAE

Subcutaneous L540cy xenografts were grown to 200 mm^3 prior to dosing with the indicated cAC10 ADCs at 3 mg/kg. After 3 days, tumors were harvested and weighed, and MMAE concentrations within the tumor homogenate were determined by LC/MS-MS. Deuterium-labeled MMAE (d8) as an internal standard was spiked into the tumor sample, followed by 1 mL of methanol. A known quantity of the tumor was homogenized with a Tissue Tearor (Biospec Products) and centrifuged. The supernatant was transferred to a 96-deep well plate and dried under a stream of nitrogen. The residual was reconstituted in 20% methanol, 0.1% formic acid, and analyzed by LC/MS-MS on a Kinetix C18 reversed phase column (Phenomenex) coupled to a Waters Quattro triple quadrupole mass spectrometer. Quantitation was performed using standards prepared from untreated tumors that were spiked with MMAE and processed in a manner identical to the samples. The density of the tumor tissue was taken to be 1.0 which was used to calculate the nanomolar concentration of MMAE within the tumor tissue.

ADC pharmacokinetic experiments

Pharmocokinetic experiments were performed using radiolabeled antibodies and ADCs. To a solution of antibody or ADC in PBS supplemented with an additional 50 mmol/L potassium phosphate (pH 8.0) and 50 mmol/L sodium chloride was added 55 μCi N10 succinimidyl propionate, [propionate-2,3-3H]- (Moravek Biochemicals, 80 Ci/mmol, 1 mCi/mL, 9:1 hexane:ethyl acetate solution) per mg of antibody or ADC. The resulting mixture was vortexed and left at room temperature for 2 hours. The mixture was centrifuged at 4,000 × *g* for 5 minutes and the lower aqueous layer was removed and split into Amicon 30-kDa MWCO Ultra-15 Centrifugal Filter Units (Millipore). Unconjugated radioactivity was removed by 4 rounds of dilution and centrifugation at 4,000 × *g*. The resulting products were filtered through sterile 0.22-μm Ultrafree-MC Centrifugal Filter Units (Millipore) and the final antibody or ADC concentration was measured spectrophotometrically. The specific activity (μCi/mg) of each product was determined by liquid scintillation counting.

The pharmacokinetic properties of the unconjugated antibody or ADC were examined in Sprague–Dawley rats. In each experiment, 3 mg of radiolabeled antibody or ADC per kg of animal weight were injected via the tail vein. Each test article was dosed once in three replicate animals. Blood was drawn into K2EDTA tubes via the saphenous vein at various time points or by cardiac puncture for terminal bleeds. Plasma was isolated by centrifugation for 10 minutes at 10,000 × *g*. A 10 to 20 μL sample of plasma from each time point was added to 4-mL Ecoscint-A liquid scintillation cocktail (National Diagnostics) and the total radioactivity was measured by liquid scintillation counting. The resulting disintegrations per minute values were converted to μCi and the specific activity of the radiolabeled test articles was used to calculate the concentration of antibody or ADC remaining in the plasma at each time point. The data were fit to a two-compartment model to derive the clearance rates using WinNonLin.

Results

Synthesis of drug-linkers

The drug-linkers were synthesized (6, 16) from the known intermediate glucuronide-MMAE (Fig. 2). Fmoc-L-Lys-OH was acylated at the ε-amine with N-hydroxysuccinimide (NHS)-activated methoxy-PEG_x reagents (or Ac_2O for drug-linker **9**) to provide Fmoc-Lys(PEG_x)-OH intermediates. The free acid was then converted to the activated ester, and subsequently reacted with glucuronide-MMAE. The lysine Nα-Fmoc was then removed under standard conditions and reacted with mDPR(Boc)-OSu to provide the penultimate intermediates. Finally, the Boc group was removed to provide mDPR-(PEG_x)-glucuronide-MMAE drug-linkers **4**-**9**. Drug-linker controls included an Nε-acetylated construct to assess the role of the lysine residue (drug-linker **9**) and a drug-linker (**10**) lacking the lysine group altogether. For drug-linker **10**, glucuronide-MMAE

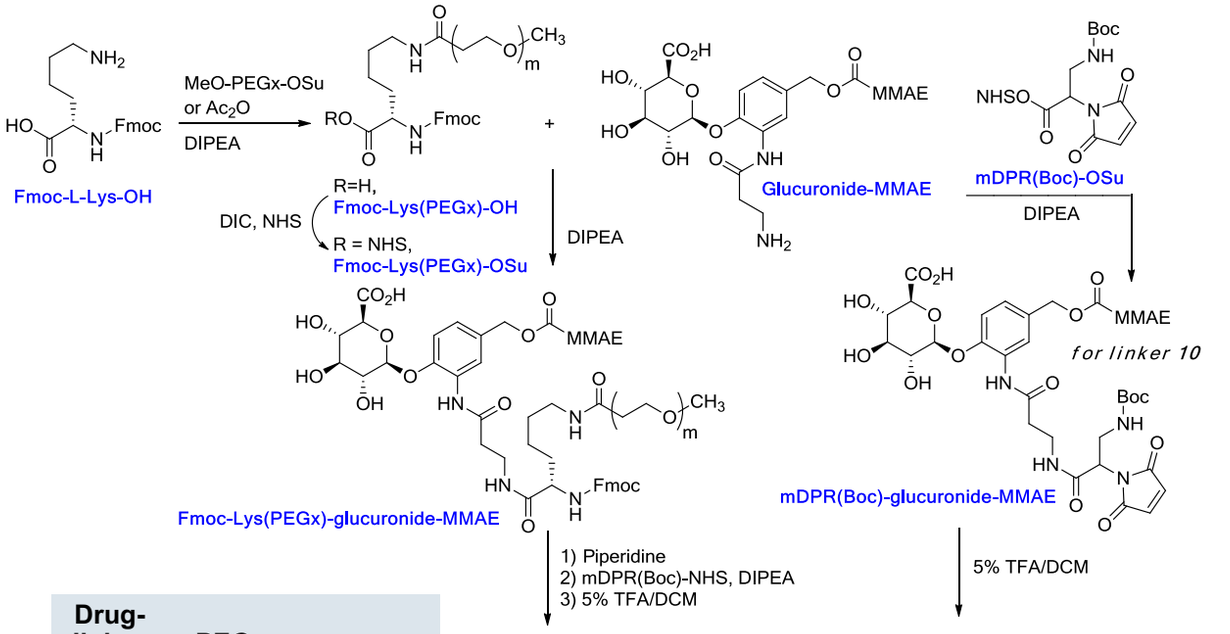

Drug-linker	PEGx	m	n
4	PEG_{24}	24	1
5	PEG_{12}	12	1
6	PEG_{8}	8	1
7	PEG_{4}	4	1
8	PEG_{2}	2	1
9	acetyl	0	1
10	No PEG	-	0

Figure 2.
General synthetic scheme to prepare mDPR-(PEG_x)-glucuronide-MMAE linkers.

was reacted directly with mDPR(Boc)-OSu to provide mDPR (Boc)-glucuronide-MMAE, which upon Boc-deprotection gave the desired product.

mDPR inclusion increases MMAE delivery *in vivo* and stability

It has previously been reported that replacement of the MC stretcher with mDPR has no effect on *in vitro* ADC potency and activity, but that the improved stability may lead to increased *in vivo* potency in a model-dependent manner (15). On the basis of these results, the impact of mDPR inclusion on intratumoral drug delivery was assessed. Mice bearing subcutaneous 200 mm^3 $CD30^+$ L540cy xenografts were administered a single intraperitoneal dose of 3 mg/kg of DAR 8 αCD30 ADCs bearing drug-linkers **2**–**4**, the tumors were harvested 3 days later, and the intratumoral drug concentration was assessed by mass spectrometry (Fig. 3). The group treated with αCD30-**2** had a lower intratumoral drug concentration of MMAE compared with αCD30-**3**, consistent with the accelerated clearance of DAR 8 ADCs comprised of drug-linker **2** (6). Finally, a modest upward trend in drug delivery over αCD30-**3** was observed with the incorporation of the self-stabilizing maleimide, as shown in αCD30-**4**. As observed previously for drug-linkers containing mDPR (15, 18), ADC bearing drug-linker **4** was highly stable over the course of 7 days at 37°C in rat plasma, whereas ADCs composed of MC-containing drug-linkers **2** and **3** underwent extensive de-conjugation under the same conditions (Supplementary Fig. S2).

***In vitro* cytotoxicity**

Anti-CD30 and αCD19 DAR 8 conjugates were tested on a panel of $CD30^+$ and $CD19^+$ cell lines. The cells were treated continuously for 96 hours and then assessed for viability. All of the drug-linkers tested provided potent and immunologically specific ADCs. On the $CD30^+$ lymphoma lines, PEG inclusion had no effect on conjugate potency, with comparable EC_{50}s observed across the cell line panel (Table 1). All αCD30 ADCs were inactive on $CD30^-$ Ramos cells, indicating a high degree of immunological specificity. The dose–response curves indicate that PEG did not impact maximal inhibition (Supplementary Fig. S3). On the $CD19^+$ Ramos and SU-DHL-4 lymphoma cell lines, the presence of PEG had minimal effect on EC_{50} potency (Table 2), whereas some variability in EC_{50} potency was observed in $CD19^+$ WSU-DLCL2 and RL cell lines. On the RL, WSU-DLCL-2, and SU-DHL-4 DLBCL cell lines the presence of larger PEGs had

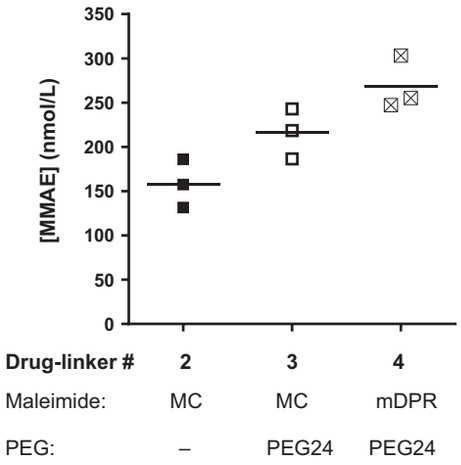

Figure 3.
Effect of mDPR inclusion on intratumoral drug delivery. Mice bearing CD30$^+$ L540cy tumors were treated with 3 mg/kg αCD30 conjugates loaded at 8 drugs/Ab. Tumors were harvested 3 days postdose and analyzed for intratumoral MMAE concentration.

an effect on maximal activity. Unlike on the Ramos Burkitt lymphoma cell line and the CD30$^+$ cell lines, the dose–response curves (Supplementary Fig. S3) revealed an attenuation in maximal cell inhibition on the DLBCL lines for the PEGylated conjugates. It is unclear why this is the case, but may be attributable to some feature of the underlying biology of the DLBCL lines that produces this result.

ADC pharmacokinetic properties and tolerability

The effects of PEG size on ADC pharmacokinetic properties were determined using drug-linkers **4–10** attached to a nonbinding IgG with a DAR of 8. Sprague–Dawley rats were administered a single intravenous dose of 3 mg/kg, and circulating antibody was monitored over time (Fig. 4A). ADC exposure increased as a function of PEG size up to PEG_8, at which point further increasing PEG size had little impact on exposure. Conjugates bearing PEG_8 or larger PEGs displayed pharmacokinetic properties approaching those of the parental antibody. The pharmacokinetic data were fit to a two-compartment model to generate pharmacokinetic parameters. Clearance as a function of PEG size is plotted in Fig. 4B. Clearance rapidly increased for all PEG conjugates bearing PEGs smaller than PEG_8 or lacking PEG entirely (drug-linkers **9** and **10**).

To evaluate the effect of ADC clearance on tolerability, Balb/C mice were administered a single dose of 50 mg/kg i.p. of DAR 8 humanized IgG1 conjugates bearing the PEG_x series on day 0 and monitored for weight loss as a function of time. As shown in Fig. 4C, ADCs bearing PEG sufficient in size to optimize pharmacokinetic exposure (PEG_8, PEG_{12}, and PEG_{24}) were well tolerated with minimal, transient weight loss observed over the course of 9 days. In contrast, ADCs bearing PEGs smaller than PEG_8 (drug-linkers **7** and **8**) or lacking PEG altogether (drug-linkers **9** and **10**) were not tolerated, with some members in each of the four groups euthanized with greater than 20% weight loss. As shown in Fig. 4D, the surviving fraction increased as pharmacokinetic exposure increased, with 100% survival for ADCs bearing PEGs sufficient to preserve exposure (PEG_8, PEG_{12}, and PEG_{24}).

After observing these tolerability differences in mice, two ADCs were selected representing both ends of the tolerability spectrum to evaluate in a more detailed study. Conjugates bearing PEG_{12} (drug-linker **5**) or lacking PEG altogether (drug-linker **10**) were again dosed at 50 mg/kg in Balb/C mice, which were sacrificed 3 days later for necropsy. Histology of the bone marrow revealed that the faster-clearing ADC prepared with drug-linker **10** resulted in substantially greater hypocellularity and hemorrhage compared to the slower clearing ADC bearing drug-linker **5** (Supplementary Fig. S4). This elevated myelosuppression was recapitulated in the hematology results, with white blood cell counts in particular being more severely depressed in animals receiving the faster-clearing ADC (Supplementary Fig. S5). Two of the three animals receiving this ADC also exhibited pronounced neutropenia. Collectively, these results suggest that bone marrow is the dose-limiting target organ of these ADCs, consistent with results published for other MMAE-containing drug-linkers (15).

In vivo xenograft models

A subset of the PEGylated drug-linkers were evaluated in a xenograft model to assess the effect of PEG size and pharmacokinetic properties on *in vivo* activity. DAR 8 αCD19 conjugates bearing PEG_{24}, PEG_{12}, PEG_8, PEG_4, and no PEG (drug-linkers **4**, **5**, **6**, **7**, and **10,** respectively) were administered to mice bearing CD19$^+$ RL diffuse large B-cell lymphoma xenografts. A single intraperitoneal dose at 3 mg/kg was given once the average tumor volume reached 100 mm^3. ADCs bearing PEG side chains sufficient in size to preserve parental antibody pharmacokinetic properties (PEG_8, PEG_{12}, and PEG_{24}) led to much more pronounced activity than faster clearing conjugates without PEG (drug-linker **10**) or with the PEG_4 (drug-linker **7**)-containing ADC. For example, αCD19-**10** displayed the most rapid clearance in the pharmacokinetic experiment and had minimal activity, whereas almost all of the animals treated with PEG_8, PEG_{12}, and PEG_{24}-containing ADCs experienced cures or complete regressions of their tumors. Thus, as in the tolerability experiment, *in vivo* activity correlated with conjugate pharmacokinetic properties, with the highest activity observed for ADCs bearing PEGs sufficient to maximize exposure.

Table 1. EC_{50} values[a] (ng ADC/mL) for αCD30 conjugates bearing PEG_x-glucuronide-MMAE linkers

		CD30$^+$ Lymphoma cell lines			
ADC	PEG_x	Karpas299, ALCL	L540cy, HL	L428, HL	Ramos, NHL (CD30$^-$)
αCD30-**4**	24	0.3 ng/mL	3	2	>1,000
αCD30-**5**	12	0.3	2	6	>1,000
αCD30-**6**	8	0.4	3	2	>1,000
αCD30-**7**	4	0.4	3	7	>1,000
αCD30-**8**	2	0.3	2	7	>1,000
αCD30-**10**	–	0.4	3	8	>1,000

[a]EC_{50} is defined here as the concentration that achieves half-maximal growth inhibition over the titration curve.

Table 2. EC_{50} values[a] (ng ADC/mL) for αCD19 conjugates bearing PEG_x-glucuronide-MMAE linkers

		CD19$^+$ lymphoma cell lines				
ADC	**PEG_x**	**Ramos, NHL**	**SU-DHL-4, DLBCL**	**WSU-DLCL2, DLBCL**	**RL, DLBCL**	**L540cy, HL (CD19$^-$)**
αCD19-**4**	24	4 ng/mL	10	2	47	>1,000
αCD19-**5**	12	2	9	17	22	>1,000
αCD19-**6**	8	3	10	39	160	>1,000
αCD19-**7**	4	3	15	2	12	>1,000
αCD19-**8**	2	2	17	7	14	>1,000
αCD19-**10**	–	2	13	4	11	>1,000

[a]EC_{50} is defined here as the concentration that achieves half-maximal growth inhibition over the titration curve.

The mDPR-(PEG_{12})-glucuronide-MMAE conjugate αCD19-**5** was further evaluated in comparison to MC-val-cit-MMAE (drug-linker **1**). Previous work has established that DAR 8 αCD30-**1** val-cit-MMAE conjugates exhibit accelerated plasma clearance, providing inferior *in vivo* activity compared with longer circulating DAR 4 conjugates (9). Therefore, the αCD19-**1** conjugate was prepared at 4-drugs/Ab, its optimal level of drug loading. Mice bearing CD19$^+$ Raji (Burkitt lymphoma) xenografts were administered a single intraperitoneal dose of conjugate on day 8 when the average tumor volume reached 100 mm^3. As shown in Fig. 5B, the DAR 8 αCD19-**5** PEG_{12}-glucuronide-MMAE conjugate dosed at 3 mg/kg achieved 10/10 cures, whereas the DAR 4 αCD19-**1** val-cit-MMAE conjugate induced only modest tumor growth delay at the same mAb dose. At a lower dose of 1 mg/kg the αCD19-**5** PEG_{12}-glucuronide-MMAE conjugate provided antitumor activity similar to the val-cit-MMAE conjugate at 3 mg/kg. Thus, the PEG_{12}-glucuronide-MMAE linker **5** provided ADC with comparable antitumor activity to those bearing val-cit-MMAE linker **1** at one-third of the antibody dose. Both drug-linkers provided inactive nonbinding conjugates (IgG-**1** and IgG-**5**) at the highest dose tested, indicating a high degree of immunologic specificity.

The conjugates were also evaluated in mice bearing CD19$^+$ WSU-DLCL2 (diffuse large B-cell lymphoma) xenografts. Mice were administered a single intraperitoneal dose on day 11 when the average tumor volume reached 100 mm^3. The DAR 8 αCD19-**5** PEG_{12}-glucuronide-MMAE conjugate dosed at 1 and 3 mg/kg induced 7/10 and 10/10 transient, complete regressions, respectively (Fig. 5C). In comparison, the DAR 4 αCD19-**1**

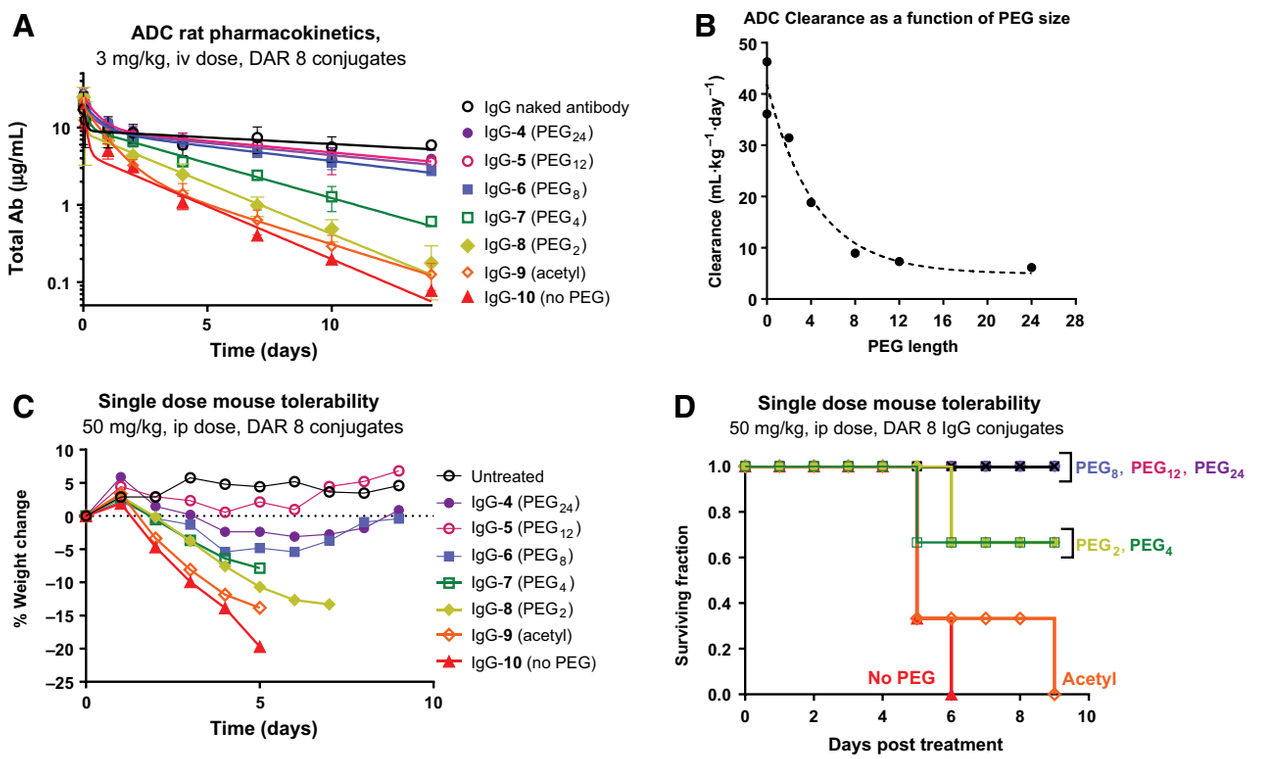

Figure 4.

ADC pharmacokinetic and tolerability as a function of PEG size. **A,** Conjugate exposure was assessed in Sprague–Dawley rats following a single intravenous dose at 3 mg/kg of ADCs bearing different size PEGs. **B,** The pharmacokinetic data were fit to a two-compartment model to derive clearance rates as a function of PEG size. Clearance rates increased rapidly for conjugates bearing PEGs smaller than PEG_8. **C,** Conjugate tolerability was assessed in Balb/C mice ($n = 3$) following a single intraperitoneal dose of PEGylated conjugates at 50 mg/kg. Conjugates bearing PEGs smaller than PEG_8 were not tolerated. Plotting was discontinued before 9 days when at least one cohort member was euthanized with greater than 20% weight loss. **D,** Mouse tolerability plotted by survival as a function of time.

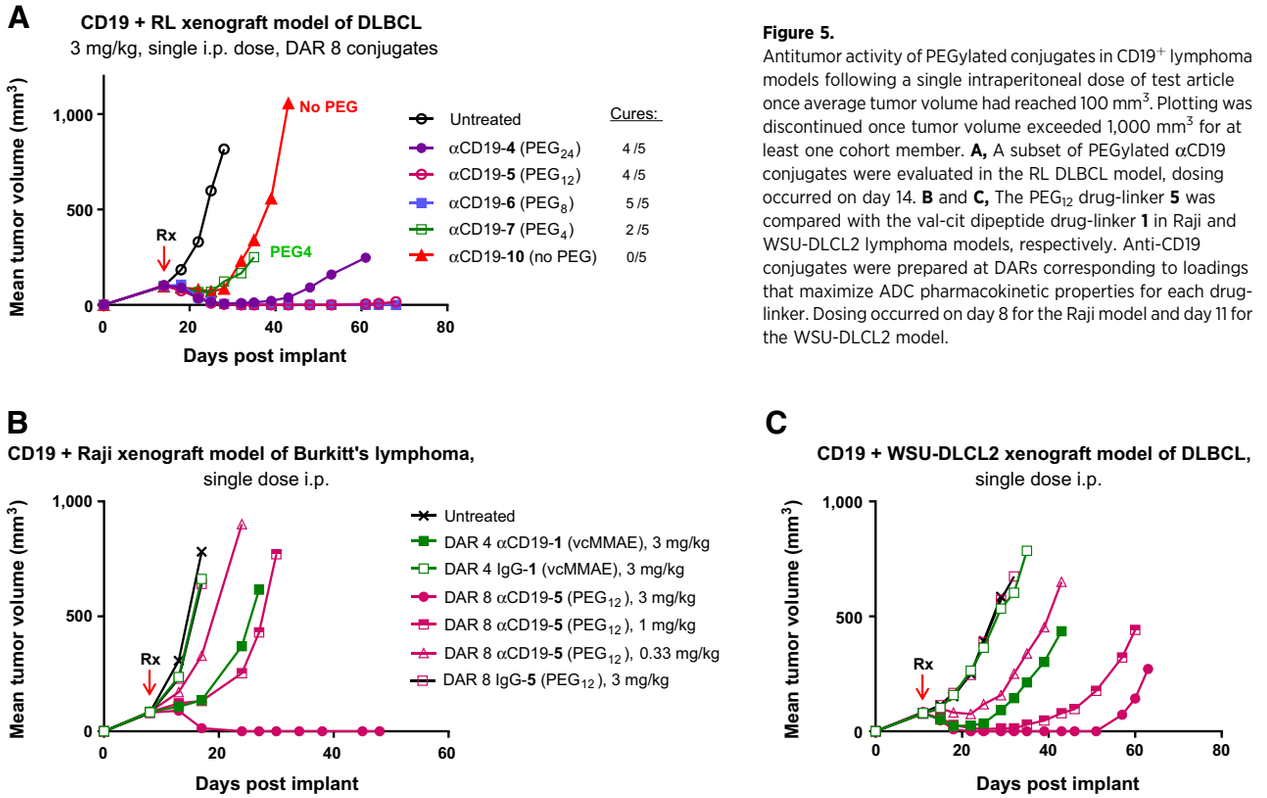

Figure 5.
Antitumor activity of PEGylated conjugates in CD19$^+$ lymphoma models following a single intraperitoneal dose of test article once average tumor volume had reached 100 mm^3. Plotting was discontinued once tumor volume exceeded 1,000 mm^3 for at least one cohort member. **A,** A subset of PEGylated αCD19 conjugates were evaluated in the RL DLBCL model, dosing occurred on day 14. **B** and **C,** The PEG_{12} drug-linker **5** was compared with the val-cit dipeptide drug-linker **1** in Raji and WSU-DLCL2 lymphoma models, respectively. Anti-CD19 conjugates were prepared at DARs corresponding to loadings that maximize ADC pharmacokinetic properties for each drug-linker. Dosing occurred on day 8 for the Raji model and day 11 for the WSU-DLCL2 model.

(val-cit-MMAE-containing conjugate) dosed at 3 mg/kg achieved 5/10 transient, complete regressions. As shown before in the Raji model, the DAR 8 PEG_{12}-gluc-MMAE conjugate displayed superior activity compared to the DAR 4 val-cit-MMAE conjugate at one-third of the antibody dose. In both cases, nonbinding IgG controls had no effect on tumor outgrowth.

Discussion

Recently, we have shown that incorporation of a PEG_{24} moiety configured in a side-chain orientation (converting drug-linker **2** to drug-linker **3**) resulted in DAR 8 conjugates with diminished nonspecific plasma clearance and consequently greater ADC exposure (6). We sought to improve upon this drug-linker through stabilization of the maleimide linkage and optimization of the size of the PEG side chain. For the purposes of maleimide stabilization, the MC- stretcher in drug-linker **3** was replaced with a self-stabilizing mDPR (drug-linker **4**), leading to a small enhancement in intratumoral drug delivery (Fig. 3). Although MC- versions of the entire PEG_x series were not evaluated, previous findings would indicate that the optimized conjugate benefits from both increased stability of the maleimide linkage (15) and increased ADC exposure by PEGylation (6). To optimize the PEG size required for the glucuronide-MMAE linker combination, a series of PEGylated constructs were synthesized, conjugated at 8 drugs/Ab, and evaluated *in vitro* and *in vivo*. On most of the lymphoma cell lines, PEG had no effect on conjugate potency. On SU-DHL-4, WSU-DLCL2, and RL DLBCL cells PEG did appear to attenuate maximal inhibition (Supplementary Fig. S3). Interestingly, the difference in maximum cell kill *in vitro* on RL cells did not appear to translate *in vivo*. In the RL xenograft model (Fig. 5A), the activity trends correlated with plasma exposure, not attenuated *in vitro* activity. It seems reasonable to surmise that pharmacokinetic effects dominate small differences in *in vitro* activity in this case.

In vivo, a clear relationship was observed between PEG size and plasma pharmacokinetics, and ultimately the therapeutic window. ADC clearance in rats decreased as PEG unit length increased up to a threshold of PEG_8, at which point larger PEGs had little impact and ADC pharmacokinetics approximated that of parental antibody (Fig. 4A). This result suggests that PEG_8 is sufficient to shield the hydrophobic moieties of the drug-linker and consequently minimize the nonspecific cellular uptake of highly loaded ADCs that we have previously documented (6). This minimization of nonspecific ADC clearance resulted in improved tolerability in a rodent model (Fig. 4C). Because ADC clearance results in the catabolic release of active drug, we postulate that the faster-clearing ADCs produce higher concentrations of drug in the tissues where nonspecific clearance is occurring, with diminished tolerability as a consequence. Conversely, results from a xenograft model (Fig. 5A) indicated greater activity was obtained with ADCs bearing PEG units sufficient in length to maximize plasma exposure. Thus, the therapeutic window appeared to benefit from both reduced toxicity and greater activity when ADC pharmacokinetics were optimized by inclusion of an appropriately sized and configured PEG chain. It is noteworthy that toxicity appears to be inversely correlated with ADC exposure, whereas antitumor activity is directly correlated with the same parameter. We believe that

this is consistent with the underlying principles of antibody-based drug delivery—that antigen-mediated uptake at the tumor is optimized by maximizing exposure to the conjugate, whereas off-target toxicity is diminished by minimizing antigen-independent ADC uptake and clearance.

Within the context of the glucuronide-MMAE linker system, PEG_8, PEG_{12}, and PEG_{24} all appeared to have the same ADC therapeutic window in rodents. Drug-linker **5**, mDPR-(PEG_{12})-glucuronide-MMAE, may be optimal for further development because it reduces by half the size of the conjugated PEG chain relative to the PEG_{24} analogue, which should lead to decreased overall hydrodynamic volume of the resulting ADC (Supplementary Fig. S1). PEG_{12} (drug-linker **5**) was prioritized over PEG_8 (drug-linker **6**) due largely to the clearance profiles shown in Fig. 4B. As PEG length decreased from PEG_8 to PEG_4 the clearance doubled from 9.0 to 18.8 mL/kg·day. In rats it appears that ADCs loaded with PEG_8-glucuronide-MMAE are perilously close to the threshold for accelerated plasma clearance. It is unknown whether the threshold for accelerated clearance would reside between PEG_4 and PEG_8 in higher species. Therefore, PEG_{12} was deemed the best option to balance PEG length reduction and mitigate the risk of interspecies differences.

We have demonstrated with a PEG_x-glucuronide-MMAE linker series that homogeneous DAR 8 ADCs with optimal ADC exposure provide a wider therapeutic window than conjugates cleared more rapidly. Furthermore, these data reinforce the concept that drug loading beyond the conventional 2–4 drugs/Ab is feasible provided payload hydrophobicity is accommodated through drug-linker design. Drug-linker **5**, mDPR-(PEG_{12})-glucuronide-MMAE, enables conjugation of MMAE to provide highly potent, homogeneous DAR 8 ADCs with a promising preclinical profile and is the subject of further investigation.

Disclosure of Potential Conflicts of Interest

No potential conflicts of interest were disclosed by the authors.

Authors' Contributions

Conception and design: P.J. Burke, R.P. Lyon
Development of methodology: P.J. Burke, J.Z. Hamilton, S.O. Doronina, N.M. Okeley
Acquisition of data (provided animals, acquired and managed patients, provided facilities, etc.): J.Z. Hamilton, J.H. Hunter, J.B. Miyamoto, M.E. Anderson, I.J. Stone, M.L. Ulrich, J.K. Simmons, E.E. McKinney
Analysis and interpretation of data (e.g., statistical analysis, biostatistics, computational analysis): P.J. Burke, J.Z. Hamilton, J.H. Hunter, J.B. Miyamoto, J.K. Simmons, R.P. Lyon
Writing, review, and/or revision of the manuscript: P.J. Burke, J.Z. Hamilton, P.D. Senter, R.P. Lyon
Administrative, technical, or material support (i.e., reporting or organizing data, constructing databases): J.B. Miyamoto, J.K. Simmons, E.E. McKinney
Study supervision: P.J. Burke, S.C. Jeffrey, E.E. McKinney, P.D. Senter

The costs of publication of this article were defrayed in part by the payment of page charges. This article must therefore be hereby marked *advertisement* in accordance with 18 U.S.C. Section 1734 solely to indicate this fact.

Received May 26, 2016; revised October 28, 2016; accepted October 31, 2016; published OnlineFirst November 9, 2016.

References

1. Senter PD, Sievers EL. The discovery and development of brentuximab vedotin for use in relapsed Hodgkin lymphoma and systemic anaplastic large cell lymphoma. Nat Biotech 2012;30:631–7.
2. Verma S, Miles D, Gianni L, Krop IE, Welslau M, Baselga J, et al. Trastuzumab emtansine for HER2-positive advanced breast cancer. New Engl J Med 2012;367:1783–91.
3. Chari RV, Miller ML, Widdison WC. Antibody-drug conjugates: an emerging concept in cancer therapy. Angewandte Chemie 2014;53:3796–827.
4. Flygare JA, Pillow TH, Aristoff P. Antibody-drug conjugates for the treatment of cancer. Chem Biol Drug Des 2013;81:113–21.
5. Senter PD. Potent antibody drug conjugates for cancer therapy. Curr Opin Chem Biol 2009;13:235–44.
6. Lyon RP, Bovee TD, Doronina SO, Burke PJ, Hunter JH, Neff-LaFord HD, et al. Reducing hydrophobicity of homogeneous antibody-drug conjugates improves pharmacokinetics and therapeutic index. Nat Biotech 2015; 33:733–5.
7. Mullard A. Maturing antibody-drug conjugate pipeline hits 30. Nat Rev Drug Discov 2013;12:329–32.
8. Doronina SO, Toki BE, Torgov MY, Mendelsohn BA, Cerveny CG, Chace DF, et al. Development of potent monoclonal antibody auristatin conjugates for cancer therapy. Nat Biotech 2003;21:778–84.
9. Hamblett KJ, Senter PD, Chace DF, Sun MM, Lenox J, Cerveny CG, et al. Effects of drug loading on the antitumor activity of a monoclonal antibody drug conjugate. Clin Cancer Res 2004;10:7063–70.
10. de Graaf M, Boven E, Scheeren HW, Haisma HJ, Pinedo HM. Beta-glucuronidase-mediated drug release. Curr Pharm Des 2002;8:1391–403.
11. Jeffrey SC, Nguyen MT, Moser RF, Meyer DL, Miyamoto JB, Senter PD. Minor groove binder antibody conjugates employing a water soluble beta-glucuronide linker. Bioorg Med Chem Lett 2007;17: 2278–80.
12. Burke PJ, Senter PD, Meyer DW, Miyamoto JB, Anderson M, Toki BE, et al. Design, synthesis, and biological evaluation of antibody-drug conjugates comprised of potent camptothecin analogues. Bioconjugate Chem 2009; 20:1242–50.
13. Jeffrey SC, Andreyka JB, Bernhardt SX, Kissler KM, Kline T, Lenox JS, et al. Development and properties of beta-glucuronide linkers for monoclonal antibody-drug conjugates. Bioconjugate Chem 2006;17:831–40.
14. Alley SC, Benjamin DR, Jeffrey SC, Okeley NM, Meyer DL, Sanderson RJ, et al. Contribution of linker stability to the activities of anticancer immunoconjugates. Bioconjugate Chem 2008;19:759–65.
15. Lyon RP, Setter JR, Bovee TD, Doronina SO, Hunter JH, Anderson ME, et al. Self-hydrolyzing maleimides improve the stability and pharmacological properties of antibody-drug conjugates. Nat Biotech 2014;32:1059–62.
16. Lyon RP, Burke PJ, Hunter JH inventors; Seattle Genetics Inc., assignee. Pegylated drug-linkers for improved ligand-drug conjugate pharmacokinetics. Patent WO 2015/057699 A2. 2015 April 23.
17. Lyon RP, Meyer DL, Setter JR, Senter PD. Conjugation of anticancer drugs through endogenous monoclonal antibody cysteine residues. Methods Enzymol 2012;502:123–38.
18. Burke PJ, Hamilton JZ, Pires TA, Setter JR, Hunter JH, Cochran JH, et al. Development of novel quaternary ammonium linkers for antibody-drug conjugates. Mol Cancer Ther 2016;15:938–45.